Multimodal classification of drug-naïve first-episode schizophrenia combining anatomical, diffusion and resting state functional resonance imaging

Huixiang Zhuang[1], Ruihao Liu[2], Chaowei Wu[2], Ziyu Meng[2], Danni Wang[2], Dengtang Liu[3], Manhua Liu[1]*, and Yao Li[2]*

[1] Dept. of Instrument Science and Engineering, School of EIEE, Shanghai Jiao Tong University, Shanghai, China

[2] Institute for Medical Imaging Technology, School of Biomedical Engineering, Shanghai Jiao Tong University, Shanghai, China

[3] Shanghai Mental Health Center, Shanghai Jiao Tong University School of Medicine, Shanghai, China

Correspondence should be addressed to:

Manhua Liu, Ph.D. Dept. of Instrument Science and Engineering, School of EIEE, Shanghai Jiao Tong University, Shanghai, 200240, China, *E-mail addresses:* mhliu@sjtu.edu.cn

Yao Li, Ph.D. Institute for Medical Imaging Technology, School of Biomedical Engineering, Shanghai Jiao Tong University, 1954 Huashan Road, Shanghai 200030, China. *E-mail addresses:* yaoli@sjtu.edu.cn

Abstract

The accurate diagnosis in the early stage of schizophrenia (SZ) is of great importance yet remains challenging. The classification between SZ and control groups based on magnetic resonance imaging (MRI) data using machine learning method could be helpful for SZ diagnosis. Increasing evidence showed that the combination of multimodal MRI data might further improve the classification performance However, medication effect has a profound influence on patients' anatomical and functional features and may reduce the classification efficiency. In this paper, we propose a multimodal classification method to discriminate drug-naïve first-episode schizophrenia patients from healthy controls by a combined structural MRI, diffusion tensor imaging (DTI) and resting state-functional MRI data. To reduce the feature dimension of multimodal data, we apply sparse coding (SC) for feature selection and multi-kernel support vector machine (SVM) for feature combination and classification. The best classification performance with the classification accuracy of 84.29% and area under the ROC curve (AUC) of 81.64% was achieved when all modality data were combined. Interestingly, the identified functional markers were mainly found in default mode network (DMN) and cerebellar connections, while the structural markers were within limbic system and prefrontal–thalamo–hippocampal circuit.

1. INTRODUCTION

The accurate diagnosis in the early stage of schizophrenia (SZ) is of great importance yet remains challenging. The brain morphological changes and functional disconnections are closely related to SZ clinical symptomology, which were revealed using structural magnetic resonance imaging (sMRI), diffusion tensor imaging (DTI) and blood oxygen level dependent (BOLD)-functional MRI (fMRI) (Teipel et al., 2015).

The classification between SZ and control groups based on MR images using machine learning method could be helpful for SZ diagnosis. Previous classification studies were mostly based on either morphological (Fan et al., 2007; Nieuwenhuis et al., 2012; Pina-Camacho et al., 2015) or functional features (Bassett et al., 2012; Guo et al., 2014a; Su et al., 2013; Yu et al., 2013a) alone. Increasing evidence showed that the combination of multimodal MRI data might further improve the classification performance of SZ (Peruzzo et al., 2015; Sui et al., 2013; Yang et al., 2016). However, the patients in the studies were all under medication, which has a profound influence on patients' anatomical and functional features and may reduce the classification efficiency (Li et al., 2012; Nieuwenhuis et al., 2012; Ren et al., 2013; Su et al., 2010; Yu et al., 2013b; Zeng et al., 2016).

In this paper, we combine multimodal MRI data, i.e. sMRI, DTI, and rs-fMRI, to perform a classification study between drug naïve first episode psychosis (FEP) patients and normal controls. To reduce the feature dimension of multimodal data, we apply sparse coding (SC) for feature selection and multi-kernel support vector machine (SVM) for feature combination and classification. We compare the classification performance using single-modal image features including cortical measures extracted from sMRI, fractional anisotropy (FA) and mean diffusivity (MD) extracted from DTI, functional connectivity (FC) and fractional amplitude of low-frequency fluctuation (fALFF) from fMRI, with those using multimodal feature combination. The most important features contributing to the classification were investigated and discussed to provide further insights into the pathophysiology of FES.

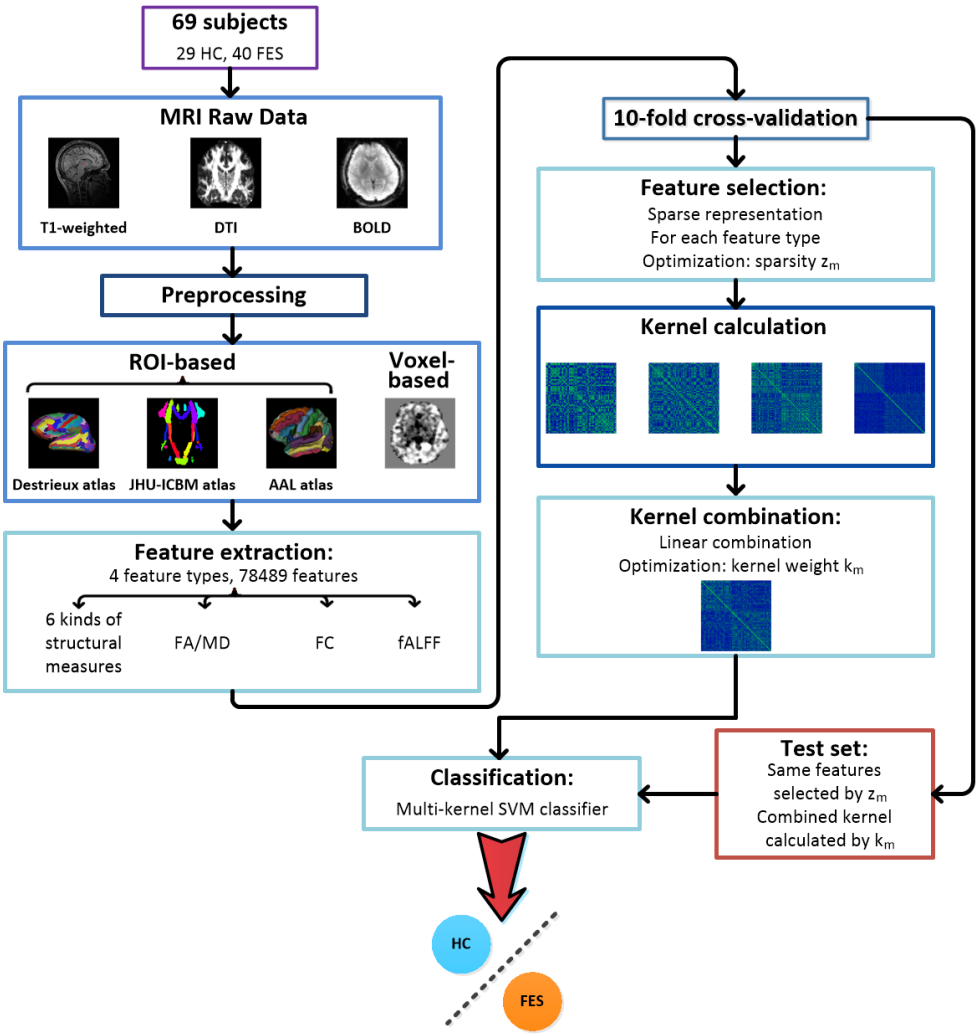

Fig.1 The framework of multimodal classification including data preprocessing, feature extraction, feature selection, multimodal combination and classification, where MRI denotes the magnetic resonance imaging and SVM denotes Support Vector Machine.

2. MATERIALS

Participants

The demographic and clinical information of the participants in our study is listed in Table 1. There are 40 drug-naïve FES patients recruited from Shanghai Mental Health Center (SMHC), China, and 29 healthy subjects matched in age, gender and education involved in this study. All patients fulfilled the Diagnostic and Statistical Manual of Mental Disorders, 4th Edition (DSM-IV) diagnosis criteria for schizophrenia confirmed by a senior psychiatrist. Exclusion criteria include substance abuse, personality disorders, mental retardation, severe cardiovascular, hepatic and renal diseases and pregnancy. All FES patients do not show any comorbid psychiatric disorders. The psychopathology and symptom severity were assessed using the positive and negative syndrome scale (PANSS). The study was approved by the Institutional Review Board of Shanghai Mental Health Center. Written informed consent was obtained from each participant.

Table 1

Demographic statistics and clinical analysis of the participants.

	Drug-naïve FES patients	Healthy Controls	P-value
Number of subjects	40	29	
Age (years)	27.13 (5.90)	27.03 (4.32)	0.909
Gender (females/males)	18/22	15/14	0.506
Education (years)	12.91 (3.14)	14.21 (2.37)	0.080
PANSS total score	73.54 (17.47)		
Course of psychosis (month)	6.51 (11.61)		

FES: First-episode schizophrenia

Data were presented with the mean score and standard deviation as mean (std).

Data Acquisition

All the MR data were collected on a 3.0-T Siemens Verio MR Scanner (Siemens AG, Erlangen, Germany) with a 32-channel head coil at SMHC. During the scanning process, all the participants were required to lay supinely with inflatable pillows placed between the head and coil to minimize motion artifacts. The participants were instructed to rest quietly with their eyes closed but to remain awake and avoid systematic thinking during scanning. The main parameters of imaging were as follows: anatomical T1-weighted images were acquired using a magnetic preparation fast gradient echo (MPRAGE) sequence with echo time (TE) = 3.65 ms, repetition time (TR) = 2530 ms, inversion time (TI) = 1100 ms, flip angle (FA) = 7°, field of view (FOV) = 256 mm, matrix size = 256 × 256, slice thickness = 1.0 mm, and slice number = 224. Blood oxygen level dependent (BOLD)-fMRI data were acquired with TE = 30 ms, TR = 2000 ms, FA = 90°, FOV = 220 mm, matrix size = 256 × 256, slice thickness = 4.0 mm, slice volume = 180, slice number = 30 and voxel size = 3.4 × 3.4 × 4.0 mm. DTI data were acquired along the AC/PC line, throughout the whole brain, with TE = 90 ms, TR = 10200 ms, FOV = 256 × 256 mm, matrix size = 128 × 128, slice thickness = 2.0 mm.

Structural MRI Data Processing

For sMRI data processing, we used Freesurfer 6.0.0 (B et al., 2004; Reuter and Fischl, 2011) and performed motion correction and conform, non-uniform (NU) intensity normalization, Talairach registration, intensity normalization, skull stripping for the following segmentation and calculation. Subcortical segmentation was subsequently performed and parcellation was conducted based on Destrieux atlas, which consists of 74 ROIs in each hemisphere. Altogether, we selected 6 different measures as our structural features (Sweeney et al., 2014), including cortical thickness, gray matter volume, surface area, mean curvature, curvature index and folding index. The total feature number of sMRI data is equal to

$$6 \times 74\ \text{ROIS} \times 2\ \text{Hemispheres} = 888\ \text{features} \quad (1)$$

DTI Processing

All DTI data were preprocessed using Pipeline for Analyzing braiN Diffusion imAges (PANDA, http://www.nitrc.org/projects/panda), which is a toolbox based on FMRIB Software Library (FSL) (Smith et al., 2004). All DICOM files were converted into NIFTI format images, followed by skull removal and eddy-current effect correction. The diffusion tensor measures including fractional anisotropy (FA) and mean diffusivity (MD) were calculated. We registered the images to the standardized template (MNI152) and the images were smoothed via a Gaussian kernel of 2 mm. Finally, we averaged the FA and MD values within 50 ROIs defined by the Johns Hopkins University white matter template. There are 100 total features, i.e., 50 for FA and 50 for MD, selected for further classification.

Resting-state fMRI Processing

fMRI data preprocessing was conducted by Data Processing Assistant for Resting-State fMRI (DPARSF v2.3, http://www.rfmri.org/DPARSF) program, which is based on Statistical Parametric Mapping 8 (SPM8, http://www.fil.ion.ucl.ac.uk/spm) and Resting-State fMRI Data Analysis Toolkit (REST v1.8, http://www.restfmri.net). First 10 volumes were removed for subjects' adaption to environment and the stabilization of the machine. The remaining 170 volumes were subsequently corrected for acquisition time with the middle slice as the reference. For individual subject, we performed head motion correction by adapting each time series to the first volume with a six-parameter and a least-square minimization linear spatial transformation. Then the functional images were normalized to standard EPI template and transformed to Montreal Neurological Institute (MNI) stereotactic space with voxel size resampled to 3x3x3 mm^3. A Gaussian kernel of 4mm full width at half-maximum (FWHM) was applied to spatially smooth the data. Further detrend was used to correct the linear drifting of signal and a temporal band-pass filter (0.01-0.08Hz) was utilized to remove the very high frequency physiological noise and low frequency drift of the fMRI data.

Functional connectivity (FC) matrices were constructed for all subjects by calculating the Pearson's correlation coefficients of mean time series in each pair of regions of interest (ROIs) based on 116 automated anatomical labeling (AAL) template. Fisher's Z transformation was further applied to FC matrices to improve the normality of the correlation coefficients. Finally, we obtained 6670 FC values as FC features for each subject

Fractional amplitude of low frequency fluctuations (fALFF) were calculated in each voxel using REST software with the following steps. Fast Fourier Transformation (FFT) were performed on band-pass (0.01-0.08Hz) filtered fMRI data to acquire the power spectrum. For each voxel, the square root of spectral power was calculated at each frequency and averaged across the entire frequency range. fALFF value was defined as the ratio of the power of each frequency within 0.01-0.08Hz to that of the whole frequency ranged from 0-0.25Hz. Then the Fisher's Z transformation was applied. In this study, fLAFF analysis was conducted within the default whole brain mask and finally we got 70831 fALFF values as features for each participant.

Feature Matrices Construction

Suppose the subject number is P, and the number of features is Q. For each feature matrix, its size can be represented as $P \times Q$. For sMRI and DTI, since the dimension of features in each modality is relatively small, we generated one matrix for each modality. For rs-fMRI, the feature dimension is relatively high. Therefore, we created for each modality a separate matrix. Finally, we

obtained 4 feature matrices from 3 modalities, which served as the inputs of the classification and regression models. To reduce the effect of unit diversity of the extracted measurements and make the multimodal features comparable, we applied the Min-Max scaling method for all features to ensure each one scaled within the range of 0 to 1 across all the subjects (Raschka, 2014).

3. Methods

After extraction of the imaging features from multimodal MRI images, we propose to apply the L1-regularzied sparse coding (SC) method for selecting the discriminant features for each modality and a multi-kernel SVM classification method to combine multimodal features for diagnosis of FES. **Fig.1** demonstrates the general framework of the proposed method.

Feature Selection based on Sparse coding

To avoid missing the important features for classification, we extracted the features as many as possible from multimodal MRI data. Thus, the total extracted multimodal features have huge dimensionality (>70000), when compared with the small number of subjects. It is necessary to develop a suitable feature selection method for the subjects to identify the discriminative features to facilitate disease classification and interpretation. Traditionally, the t-test method is used to find significant biomarkers by individually evaluating the discrimination of each feature with p-value. However, this method has completely ignored the correlation of imaging features and failed to consider the discrimination of multiple variable combination. This is not suitable for our application because informative imaging biomarkers may be distributed over more than one brain region. Thus, to identify the informative imaging biomarkers, a multivariate model is learned to consider the combination of features over the distant brain regions for handling the multivariate interactions in feature selection. Sparse coding (SC), also called sparse representation, as a machine learning method, has been widely applied to the task of feature selection (Lai et al., 2009; Lan et al., 2010), as well as classification (Lai and Jiang, 2016; Wright et al., 2009) in the field of face recognition. In this work, a sparse coding method with $L1$-regularization (Ghosh and Chinnaiyan, 2005; Tibshirani, 2011) was applied to select the informative features for each modality. Unlike the traditional two-sample t-test, SC considers the combination of multi-variable features to achieve a global significance.

Let $\mathbf{A}$ represents a $P \times Q$ feature matrix where P and Q are the numbers of subjects and features in the matrix, respectively. The *p-th* row of $\mathbf{A}$ is the feature vector of the image from the *p-th* participant. y denotes the class label of all participants with the *p-th* element being the class label of the *p-th* participant. Thus, a linear regression model can be used to generate the class outputs with a set of features as follows:

$$\mathrm{y} = \mathbf{A}\vec{\omega} + \varepsilon \tag{2}$$

where $\vec{\omega} = \left(\omega_1, \omega_2, \dots, \omega_Q\right)^T$ is a vector of coefficients assigned to the corresponding features, and ε is an independent error term. The class output can be characterized as the linear combination of the features. One popular method to solve this problem is the least square optimization. When the

number of extracted features is large, $L1$-regularized sparsity is imposed on the coefficients to choose a small number of relevant and discriminant features for classification. The $L1$-regularized least square problem, also called as Lasso problem, can be formulated as:

$$\vec{\omega} = \text{argmin}_{\omega} \|y - \mathbf{A}\vec{\omega}\|_2^2 + \text{z}\|\vec{\omega}\|_1, \;\; s.t. \;\; \vec{\omega}_i \geq 0, \forall i \tag{3}$$

where z is the sparsity regularization parameter which controls the amount of zero coefficients in $\vec{\omega}$. The non-zero element in $\vec{\omega}$ indicates that the corresponding feature is more relevant to the classification. When the z value increases, the number of non-zero elements in $\vec{\omega}$ decreases, and more features will be selected to be relevant. Thus, the $L1$-regularized SC method provides an effective multivariate regression model to select a subset of relevant features by taking into consideration both the correlation of features to the class label and the combinations of individual features (Liu et al., 2014). By adjusting the values of sparsity, various number of features can be selected without ranking. This method can jointly select the features from multiple contiguous brain regions based on the population difference. However, SC cannot work well for multimodal classification since different modality features have different discriminability. How to effectively combine the multimodal features for classification is still challenging. Thus, we propose to apply the multi-kernel SVM for multimodal classification.

Multimodal Classification

We applied the multi-kernel support vector machine (MKL-SVM) classifier to combine the multimodal features for classification. Different from conventional linear classifier, the kernel-based SVM classifier maps the linearly non-separable features in the original lower-dimension space to a higher dimension feature space, where they are more likely to be separable with a kernel function. In the higher dimension space, a maximum margin hyperplane is calculated with SVM for classification. To combine the multimodal features $M = \{\text{sMRI, DTI, FC, fALFF}\}$, MKL-SVM solves the primal problem (Zhang et al., 2011b):

$$\begin{gathered} \min_{\omega^m, b, \xi_i} \;\; \frac{1}{2}\sum\nolimits_{m\in M} \beta_m \|\omega^m\|^2 + C\sum_{i=1}^{P} \xi_i \\ s.t. \;\; y_i\left(\sum\nolimits_{m\in M} \beta_m((\omega^m)^T \phi^m(x_i^m) + b)\right) \geq 1 - \xi_i \\ \xi_i \geq 0, i = 1, \ldots, P. \end{gathered} \tag{4}$$

where $\omega^m, \phi(x_i)$ are the normal vector of hyperplane and the kernel-induced mapping function, respectively; x_i^m and $\beta_m \in [0,1]$ are the feature vector of m-modality and the weight assigned to the feature of m-modality; y_i is the class label of subject *i*; The dual form of MKL-SVM is defined as:

$$\max_{\alpha} \;\; \sum_{i=1}^{P} \alpha_i - \frac{1}{2}\sum_{i=1}^{P}\sum_{j=1}^{P} \alpha_i \alpha_j y_i y_j \left[\sum\nolimits_{m\in M} \beta_m K\left(x_i^m, x_j^m\right)\right] \tag{5}$$

$$s.t. \quad \sum_{i=1}^{P} \alpha_i y_i = 0, \qquad 0 \le \alpha_i \le C, i = 1, \dots, P$$

where $K(x_i^m, x_j^m)$ is the kernel function for two training subjects on the m-modality and the cost parameter C is set to 1. A mixed kernel $K(x_i, x_j) = \sum_{m \in M} \beta_m K(x_i^m, x_j^m)$ is obtained by a weighted combination of the multiple kernels generated from multimodal features. We constrain $\sum_{m \in M} \beta_m = 1$ and use a coarse-grid search through cross-validation on the training samples to obtain the optimal weights. For a new test sample, the output (predicted labels) of MKL-SVM can be generated as below:

$$f(x) = sign\left\{\sum_{i=1}^{P} \alpha_i y_i \left[\sum\nolimits_{m \in M} \beta_m K(x_i^m, x^m) + b\right]\right\} \tag{6}$$

In our implementation, the LIBSVM toolbox (Chang and Lin, 2011) is used to implement the SVM classifier with the mixed kernel matrix for the multi-modal classification tests.

4. Results and Discussion

To evaluate the classification performance, the 10-fold cross-validation was performed. Each time the 9-fold data were used for training and 1 fold for testing. In the experiment, the parameters to be optimized are sparsity z, which can be adjusted to change the number of selected features, and the weights $\beta_m, m \in M$. Grid search was used to optimize the parameters from 0 to 1 at step of 0.05 for z and from 0 to 1 at step of 0.1 for β_m.

The classification accuracy, sensitivity and specificity, were calculated as follows:

$$\text{accuracy} = \frac{\text{TN} + \text{TP}}{\text{TN} + \text{FP} + \text{FN} + \text{TP}} \% \tag{7}$$

$$\text{sensitivity} = \frac{\text{TP}}{\text{FN} + \text{TP}} \% \tag{8}$$

$$\text{specificity} = \frac{\text{TN}}{\text{TN} + \text{FP}} \% \tag{9}$$

where TP is the number of FES patients correctly classified, TN is the number of HCs correctly predicted, FP denotes the number of HCs falsely classified, and FN is the number of falsely classified FES patients. Thus, the sensitivity denotes the accuracy to classify patients while the specificity evaluates the accuracy to classify healthy controls. In addition, ROC curve was demonstrated by sensitivity and 1-specificity at different thresholds and area under the ROC curve (AUC) was calculated to further evaluate the classification performance (Huang and Ling, 2005; Ling et al., 2003). We will present the classification results of single/multi-modality and discuss the selected biomarkers in the following.

Single-modal Classification

We firstly test the classification performance with single modality. There are 4 types of features (denoted as sMRI, DTI, FC, fALFF) extracted from 3 MRI modalities: sMRI, DTI and fMRI. Table 2 compares the classification performance and feature number of each modality as well as multimodal classification. The comparison of the corresponding ROC curves is also demonstrated in Fig.2. From these results, we can see that FC feature of rs-fMRI can achieve the best single-modal

classification result with accuracy at 75.24% and AUC at 75.26%. The fALFF and DTI features have relatively lower discriminative capability. Table 2 also presents the dimension of selected features (the input of classifier) before and after using SC. We can see that SC can effectively identify the informative features and improve the classification performance. Subjects can be correctly classified with less than 5% features selected by SC, which indicates that a large number of imaging features are redundant for classification.

Table 2 Classification results of first-episode schizophrenia patients and healthy controls. The classification performance is evaluated by accuracy, sensitivity, specificity, AUC on both single modal and multimodal combination. Both SVM and SC+SVM were conducted and compared. # represents the dimension of features participated in SVM classifier.

Feature	Accuracy (%)	Sensitivity (%)	Specificity (%)	AUC (%)	# of features
sMRI	61.43	85.00	30.00	54.66	888
	71.19	77.50	63.33	68.19	4
DTI	60.48	65.00	53.33	50.60	100
	67.86	72.50	61.67	63.45	9
FC	74.05	82.50	63.33	74.48	6670
	75.24	80.00	68.33	**75.26**	39
fALFF	60.71	80.00	35.00	56.29	70831
	69.29	80.00	55.00	61.90	1662
Multimodal	76.67	95.00	58.33	42.84	78489
	84.29	92.50	73.33	**81.64**	1714

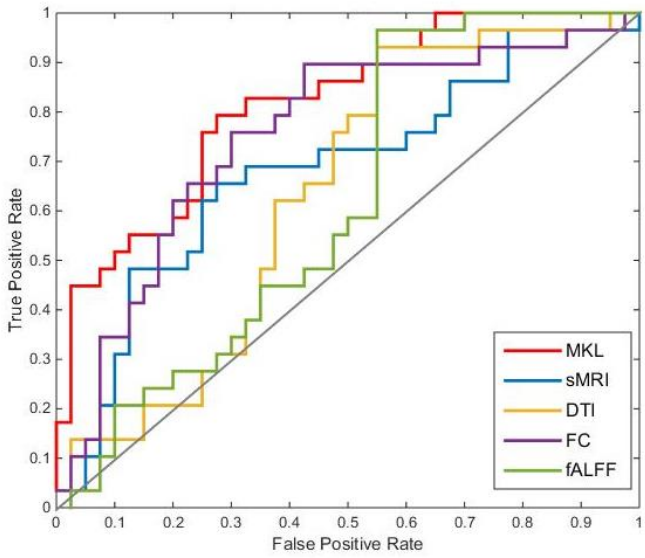

Fig.2 ROC curves for classification of FES and HC on 4 different MRI feature types (sMRI, DTI, FC and fALFF) and their multimodal combination via SC+SVM. MKL: multimodal classification by multi-kernel linear SVM. The gray diagonal line denotes random classification result.

Multimodal Classification

The performance of multimodal classification is better than any single modal one, with 84.29% accuracy and 81.64% AUC, showing that the combination of multiple modalities by our proposed method significantly improves the classification performance. Moreover, Table 3 and Table 4 show the results of classification accuracy and AUC, respectively, with different combinations of multiple MRI modalities. The experiments were performed by gradually adding a new type of feature. From these results, we can see that the classification performance improved by combing sMRI with DTI. When the features of FC and fALFF were further added to the sMRI+DTI combination, the classification performance improved further and reached the best when combining all modal features together. These results indicate that adding an extra modality feature could improve the classification performance while multimodal features achieve the best classification performance for disease diagnosis.

Table 3 The comparison of classification accuracy with different combinations of multiple feature types. Step 1, 2, 3, 4 indicate gradually including multimodal features into the combination.

Step\Combined:	sMRI (%)	DTI (%)	FC (%)	fALFF (%)
1:-	71.19	67.86	75.24	69.29
2:sMRI	-	74.29	75.71	74.05
3:sMRI+DTI	-	-	78.57	75.48
4:sMRI+DTI+FC	-	-	-	**84.29**

Table 4 The comparison of AUC with different combinations of multiple feature types. Step 1, 2, 3, 4 indicate gradually including multimodal features into the combination.

Step\Combined:	sMRI (%)	DTI (%)	FC (%)	fALFF (%)
1:-	68.19	63.45	75.26	61.90
2:sMRI	-	68.97	75.52	68.45
3:sMRI+DTI	-	-	79.31	73.02
4:sMRI+DTI+FC	-	-	-	**81.64**

Biomarker Identification

We examined the selected multimodal features by SC with the optimal regularization parameter for single-modal classification. In our experiment, the standard 10-fold CV was used. The selected features are different for different folds. Thus, we compute the frequency of features selected in 10 folds and select the imaging features with frequency higher than 5 as the identified biomarkers. Table 5 listed the identified sMRI and DTI biomarkers. Fig.3 showed the identified regions for DTI data. Fig. 4 demonstrated the identified FC biomarkers from fMRI data.

For the biomarkers of sMRI data as shown in Table 5, the identified biomarkers inculde the cortical thickness in the left superior segment of the circular sulcus of the insula, the mean curvature of left temporal plane of the superior temporal gyrus (STG), the curvature index of left posterior transverse collateral sulcus, and right long insular gyrus and central sulcus of the insula.

For DTI biomarker, the FA changes are within left superior corona radiata, left fornix, left posterior thalamic radiation. The MD changes are in right uncinate fasciculus (UF), right superior cerebellar peduncle, right posterior thalamic radiation (include optic radiation), right cingulum (cingulate gyrus). Both FA and MD in right cingulum (hippocampus) were identified as the significant biomarkers.

For the biomarkers of FC results, the connection map is depicted in Fig.4. We find the most discriminant FCs include: sub-regions in cerebellar lobe with both internal connections and to the cortical regions; STG to thalamus and cerebellar regions; right parahippocampal gyrus (PHG) to left calcarine and bilateral lingual gyrus; bilateral postcentral gyrus (PoCG) and paracentral lobe (PCL) to bilateral thalamus, caudate, and cerebellar regions. For the biomarkers of fALFF results, the most related fALFF voxels mainly located in bilateral occipital lobe, precuneus, and cuneus. Other smaller regions include left angular gyrus (ANG), bilateral lingual gyrus, calcarine, and cerebellar regions.

Table 5 The most identified sMRI and DTI biomarkers. During classification procedure, the features selected in 10 folds of cross validation with optimal sparsity were recorded. The features selected with frequency over 5 in 10-fold cross validation were listed.

	Brain Region	Feature	Hemisphere
sMRI			
No.49	Superior segment of the circular sulcus of the insula	Thickness	Left
No.36	Planum temporale or temporal plane of the superior temporal gyrus	Mean curvature	Left
No.51	Posterior transverse collateral sulcus	Curvature index	Left
No.17	Long insular gyrus and central sulcus of the insula	Curvature index	Right
DTI			
No.26	Superior corona radiate	FA	Left
No.40	Fornix	FA	Left
No.37	Cingulum (hippocampus)	FA, MD	Right
No.47	Uncinate fasciculus	MD	Right
No.30	Posterior thalamic radiation (include optic radiation)	FA	Left
No.29	Posterior thalamic radiation (include optic radiation)	MD	Right
No.13	Superior cerebellar peduncle	MD	Right
No.35	Cingulum (cingulate gyrus)	MD	Right

Discussion

In this paper, we propose a multimodal classification method to discriminate first-episode schizophrenia patients from healthy controls by a combined structural MRI, DTI and resting state-functional MRI data. The features extracted included morphological measurements in both gray matter and white matter, functional connectivity and regional functional activity. We proposed a classification method composed of sparse coding and multi-kernel SVM, in which SC was applied for feature selection and SVM was used for multimodal classification. The best classification

performance was achieved when all modalities were combined. More specifically, the structural varieties were shown in limbic system and prefrontal–thalamo–hippocampal circuit, while the functional abnormality was mainly found in default mode network (DMN) and FCs linked to cerebellar, parietal and temporal lobes.

To the best of our knowledge, this is the first study for drug-naïve first-episode schizophrenia (FES) patients classification using a combined sMRI, fMRI and DTI technology. The effects of antipsychotic treatment on FES patients' anatomical and functional changes have been widely reported in previous literature (Cahn et al., 2002; Lui et al., 2010; Wang et al., 2013; Zeng et al., 2016). Though the elimination of pharmaceutical effect is important to understand the pathophysiology of FES, there are very few studies conducted for machine learning-based drug-naïve FES patients classification, due to the difficulty of patients recruitment (Organization, 1993). Peruzzo et al. applied MKL and SVM to combined sMRI and DTI data from medicated FES patients, and found that the best classification performance was achieved by the integration of multimodal imaging information. In this study, a relatively small sample size (23 vs 23) was used, also the number of features was much less (442) compared to our study (78489) because of the lack of functional data. Functional network alteration plays an important role in the detection of early-onset brain changes, which often takes place before the morphological changes (Teipel et al., 2015). Sui et al. used a voxel-wise analysis and combined features from sMRI, DTI and rs-fMRI data and achieved a classification accuracy of 79%. However, the patients included in this study were not all first-episode schizophrenia. In our study, combining features from sMRI, fMRI and DTI data, we utilized a multi-kernel SVM classifier and reached the highest accuracy over 84% in classification of drug naïve FES patients.

Recently, increasing number of studies improved the classification performance by using multi-modality data in a variety of mental disorders including SZ and Alzheimer's disease (Dyrba et al., 2015; Wee et al., 2012; Zhang et al., 2011a). For multimodal data, the feature dimension significantly increases and overfitting problem is more prominent. For dimension reduction, a variety of methods including principal component analysis (PCA), independent component analysis (ICA) and linear discriminant analysis (LDA), were applied to improve the multimodal classifier performance (Richard et al., 2013; Song et al., 2017; Wang et al., 2013). Through dimensionality reduction, the feature information was represented in a lower dimension. Another way to reduce information redundancy is by feature selection, for which filter, wrapper, and embedding are widely applied methods (Cao et al., 2016; Shen et al., 2010; Sui et al., 2014). In our study, we applied SC for feature selection in our classification method. From the large number of features, SC eliminate most redundant features and combine the critical features for prediction. For FES auto-diagnosis by multimodal MR data, the small number of biomarkers selected by SC make the disease easier to interpret. Compared to other traditional methods, SC has been proved to achieve optimal selection of multiple features related to the classification task instead of separately considering the significant features. In our study, significant improvements in classification performance was shown when SC was applied for feature selection of multimodal imaging data. The improvements were presented for various feature dimensions ranged from 100 to 78489, as shown in Table 2. This provides a proof of the effectiveness of SC for feature selection in the integration of multimodal MRI data to improve the classification performance.

For functional feature, the FC contributed most to the discrimination, among which the FCs from cerebellar area to cortical regions were the most identified ones. This finding is in line with previous SZ studies (Andreasen and Pierson, 2008; Collin et al., 2011; Kasparek et al., 2012). A recent study first reported functional abnormality in the cerebellum of drug-naïve FES patients (Guo et al., 2018). Cerebellum plays an important role in conceptual activity and emotion state as well as motor control (Schmahmann, 2001). Besides the cerebellar system, the medial temporal area within DMN also contributed to the classification in our study, including bilateral parahippocampal gyrus, precuneus and angular gyrus (Guo et al., 2017; Guo et al., 2014b; He et al., 2013; Wang et al., 2016). Medial temporal area function was related with autobiographical memory in SZ patients (Andrews-Hanna et al., 2014). We suggest that the syndromes caused by these functional network impairments are significantly related to early onset schizophrenia. The structural changes found in our study were mainly in the limbic system such as the insula area. While the biomarkers from DTI modality were related to fibers for memory such as UF, fornix, and hippocampus. The prefrontal–thalamo–hippocampal circuit, as a well identified pathway in working memory (Bolkan et al., 2017; Marenco et al., 2012), has been reported closely related with SZ pathophysiology (Caprihan et al., 2015; Domen et al., 2013; Fitzsimmons et al., 2009; Poletti et al., 2015; Zhou et al., 2008).

To summarize, the functional and structural biomarkers that we found to discriminate drug naïve FES patients have showed different regional characteristics. The functional features were mostly network connectivity to cerebellum and DMN, while structural features largely located in the limbic system and memory related circuits.

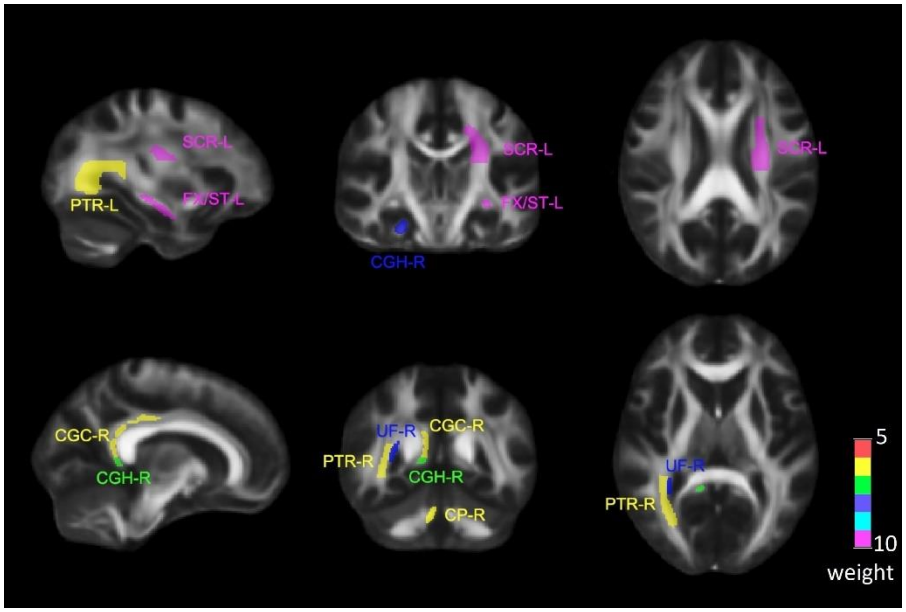

Fig.3 The most identified ROIs in DTI data overlaid on JHU-ICBM white matter atlas. They were depicted in 6 tomographic images from 3 coordinates: The axial plane (z-plane), the coronal plane (y-plane), and the sagittal plane (x-plane). Top row: Significant FA ROIs biomarkers. Bottom row: Significant MD ROIs biomarkers. PTR-L= Left posterior thalamic radiation, SCR-L= Left superior corona radiata, CGH-R = Right cingulum (hippocampus), FX/ST-L = Left fornix/stria terminalis, CGC-R = Right cingulum (cingulate gyrus), PTR-R = Right posterior thalamic radiation, UF-R = Right uncinate fasciculus, CP-R = Right cerebral peduncle

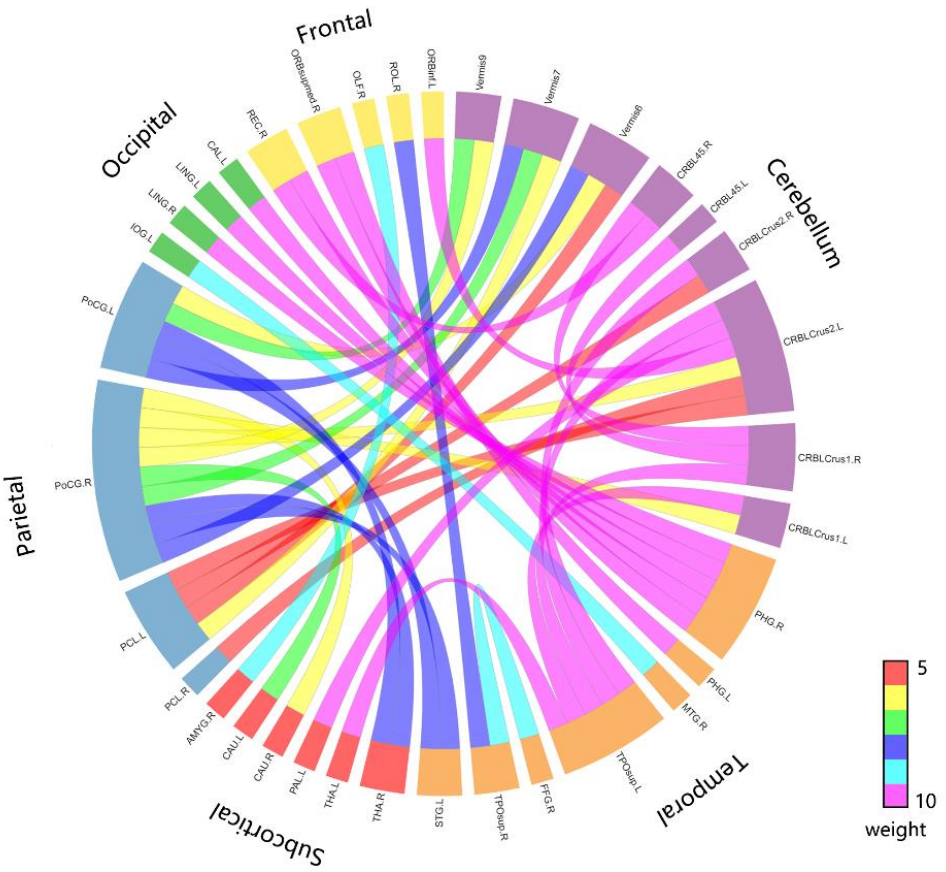

Fig.4 The connectivity map of top FC features. The labels on the circle denote the ROIs in AAL atlas as nodes in FCs. The edges are presented by bands with different colors that associated with the frequency.

5. Conclusion

In this paper, we have proposed a multimodal classification framework using multi-kernel and sparse coding machine learning method for discriminating drug naïve FES patients and heathy controls. We combine multimodal MR imaging data, including structural MR images, diffusion tension images and resting-state functional MR images. To effectively increase the performance of SVM classifier, we applied sparse coding to filter out the large number of features to identify the most discriminative image biomarkers. The best classification performance was achieved when incorporating all anatomical, diffusion weighted and resting state fMRI images for drug naïve FES patients. The identified functional markers mostly related to DMN and cerebellar connections, and the structural markers were within limbic system and memory related fibers.

References

Andreasen, N.C., Pierson, R., 2008. The Role of the Cerebellum in Schizophrenia. Biological Psychiatry 64, 81-88.

Andrews-Hanna, J.R., Smallwood, J., Spreng, R.N., 2014. The default network and self-generated

thought: component processes, dynamic control, and clinical relevance. Annals of the New York Academy of Sciences 1316, 29.

B, F., DH, S., AJ, v.d.K., N, M., F, S., BT, Q., AM, D., 2004. Sequence-independent segmentation of magnetic resonance images. Neuroimage 23 Suppl 1, S69.

Bassett, D.S., Nelson, B.G., Mueller, B.A., Camchong, J., Lim, K.O., 2012. Altered resting state complexity in schizophrenia. Neuroimage 59, 2196-2207.

Bolkan, S.S., Stujenske, J.M., Parnaudeau, S., Spellman, T.J., Rauffenbart, C., Abbas, A.I., Harris, A.Z., Gordon, J.A., Kellendonk, C., 2017. Thalamic projections sustain prefrontal activity during working memory maintenance. Nature Neuroscience 20.

Cahn, W., Hulshoff Pol, H.E., Lems, E.B., van Haren, N.E., Schnack, H.G., Ja, V.D.L., Schothorst, P.F., Van, E.H., Kahn, R.S., 2002. Brain volume changes in first-episode schizophrenia: a 1-year follow-up study. Archives of General Psychiatry 59, 1002.

Cao, T.T., Zhang, M., Andreae, P., Xue, B., 2016. A Wrapper Feature Selection Approach to Classification with Missing Data. European Conference on the Applications of Evolutionary Computation, pp. 685-700.

Caprihan, A., Jones, T., Chen, H., Lemke, N., Abbott, C., Qualls, C., Canive, J., Gasparovic, C., Bustillo, J.R., 2015. The Paradoxical Relationship Between White Matter, Psychopathology and Cognition in Schizophrenia: A Diffusion Tensor and Proton Spectroscopic Imaging Study. Neuropsychopharmacology 40, 2248.

Chang, C.C., Lin, C.J., 2011. LIBSVM: A library for support vector machines. Acm Transactions on Intelligent Systems & Technology 2, 1-27.

Collin, G., Pol, H.E.H., Haijma, S.V., Cahn, W., Kahn, R.S., Heuvel, M.P.V.D., 2011. Impaired Cerebellar Functional Connectivity in Schizophrenia Patients and Their Healthy Siblings. Front Psychiatry 2, 73.

Domen, P.A., Michielse, S., Gronenschild, E., Habets, P., Roebroeck, A., Schruers, K., Van, O.J., Marcelis, M., 2013. Microstructural white matter alterations in psychotic disorder: a family-based diffusion tensor imaging study. Schizophrenia Research 146, 291.

Dyrba, M., Grothe, M., Kirste, T., Teipel, S.J., 2015. Multimodal analysis of functional and structural disconnection in Alzheimer's disease using multiple kernel SVM. Hum Brain Mapp 36, 2118-2131.

Fan, Y., Shen, D., Gur, R.C., Gur, R.E., Davatzikos, C., 2007. COMPARE: classification of morphological patterns using adaptive regional elements. IEEE transactions on medical imaging 26, 93-105.

Fitzsimmons, J., Kubicki, M., Smith, K., Bushell, G., Estepar, R.S., Westin, C.F., Nestor, P.G., Niznikiewicz, M.A., Kikinis, R., Mccarley, R.W., 2009. Diffusion tractography of the fornix in schizophrenia. Schizophrenia Research 107, 39-46.

Ghosh, D., Chinnaiyan, A.M., 2005. Classification and selection of biomarkers in genomic data using LASSO. Journal of Biomedicine & Biotechnology 2005, 147.

Guo, W., Liu, F., Chen, J., Wu, R., Li, L., Zhang, Z., Chen, H., Zhao, J., 2017. Hyperactivity of the default-mode network in first-episode, drug-naive schizophrenia at rest revealed by family-based case-control and traditional case-control designs. Medicine 96, e6223.

Guo, W., Su, Q., Yao, D., Jiang, J., Zhang, J., Zhang, Z., Yu, L., Zhai, J., Xiao, C., 2014a. Decreased regional activity of default-mode network in unaffected siblings of schizophrenia patients at rest. European Neuropsychopharmacology 24, 545.

Guo, W., Yao, D., Jiang, J., Su, Q., Zhang, Z., Zhang, J., Yu, L., Xiao, C., 2014b. Abnormal default-mode network homogeneity in first-episode, drug-naive schizophrenia at rest. Prog Neuropsychopharmacol Biol Psychiatry 49, 16-20.

Guo, W., Zhang, F., Liu, F., Chen, J., Wu, R., Chen, D.Q., Zhang, Z., Zhai, J., Zhao, J., 2018. Cerebellar abnormalities in first-episode, drug-naive schizophrenia at rest. Psychiatry Research.

He, Z., Deng, W., Li, M., Chen, Z., Jiang, L., Wang, Q., Huang, C., Collier, D.A., Gong, Q., Ma, X., 2013. Aberrant intrinsic brain activity and cognitive deficit in first-episode treatment-naive patients with schizophrenia. Psychological Medicine 43, 769-780.

Huang, J., Ling, C.X., 2005. Using AUC and accuracy in evaluating learning algorithms. IEEE Transactions on Knowledge & Data Engineering 17, 299-310.

Kasparek, T., Rehulova, J., Kerkovsky, M., Sprlakova, A., Mechl, M., Mikl, M., 2012. Cortico-cerebellar functional connectivity and sequencing of movements in schizophrenia. BMC Psychiatry,12,1(2012-03-12) 12, 17.

Lai, J., Jiang, X., 2016. Class-wise Sparse and Collaborative Patch Representation for Face Recognition. IEEE Trans Image Process 25, 3261-3272.

Lai, Z., Jin, Z., Yang, J., 2009. Global Sparse Representation Projections for Feature Extraction and Classification. Pattern Recognition, 2009. CCPR 2009. Chinese Conference on, pp. 1-5.

Lan, C., Jing, X.Y., Li, S., Bian, L.S., Yao, Y.F., 2010. Exploring the natural discriminative information of sparse representation for feature extraction. International Congress on Image and Signal Processing, pp. 916-920.

Li, M., Chen, Z., Deng, W., He, Z., Wang, Q., Jiang, L., Ma, X., Wang, Y., Chua, S.E., Cheung, C., 2012. Volume increases in putamen associated with positive symptom reduction in previously drug-naive schizophrenia after 6 weeks antipsychotic treatment. Psychological Medicine 42, 1475-1483.

Ling, C.X., Huang, J., Zhang, H., 2003. AUC: a statistically consistent and more discriminating measure than accuracy. Proceedings of the 18th international joint conference on Artificial intelligence, pp. 519--524.

Liu, M., Zhang, D., Shen, D., 2014. Identifying informative imaging biomarkers via tree structured sparse learning for AD diagnosis. Neuroinformatics 12, 381-394.

Lui, S., Li, T., Deng, W., Jiang, L., Wu, Q., Tang, H., Yue, Q., Huang, X., Chan, R.C., Collier, D.A., 2010. Short-term effects of antipsychotic treatment on cerebral function in drug-naive first-episode schizophrenia revealed by "resting state" functional magnetic resonance imaging. Archives of General Psychiatry 67, 783.

Marenco, S., Stein, J.L., Savostyanova, A.A., Sambataro, F., Tan, H.Y., Goldman, A.L., Verchinski, B.A., Barnett, A.S., Dickinson, D., Apud, J.A., 2012. Investigation of Anatomical Thalamo-Cortical Connectivity and fMRI Activation in Schizophrenia. Neuropsychopharmacology Official Publication of the American College of Neuropsychopharmacology 37, 499.

Nieuwenhuis, M., van Haren, N.E., Hulshoff Pol, H.E., Cahn, W., Kahn, R.S., Schnack, H.G., 2012. Classification of schizophrenia patients and healthy controls from structural MRI scans in two large independent samples. Schizophrenia Research 136, S205-S205.

Organization, W.H., 1993. The ICD-10 Classification of Mental and Behavioural Disorders: Clinical Description and Diagnostic Guidelines. World Health Organization.

Peruzzo, D., Castellani, U., Perlini, C., Bellani, M., Marinelli, V., Rambaldelli, G., Lasalvia, A., Tosato, S., De Santi, K., Murino, V., Ruggeri, M., Brambilla, P., 2015. Classification of first-episode psychosis: a multi-modal multi-feature approach integrating structural and diffusion imaging. J Neural Transm (Vienna) 122, 897-905.

Pina-Camacho, L., Garcia-Prieto, J., Parellada, M., Castro-Fornieles, J., Gonzalez-Pinto, A.M., Bombin, I., Graell, M., Paya, B., Rapado-Castro, M., Janssen, J., 2015. Predictors of schizophrenia spectrum

disorders in early-onset first episodes of psychosis: a support vector machine model. European Child & Adolescent Psychiatry 24, 427-440.

Poletti, S., Mazza, E., Bollettini, I., Locatelli, C., Cavallaro, R., Smeraldi, E., Benedetti, F., 2015. Adverse childhood experiences influence white matter microstructure in patients with schizophrenia. Psychiatry Res 234, 35-43.

Raschka, S., 2014. About Feature Scaling and Normalization and the effect of standardization for machine learning algorithms. Polar Political & Legal Anthropology Review 30, 67-89.

Ren, W., Lui, S., Deng, W., Li, F., Li, M., Huang, X., Wang, Y., Li, T., Sweeney, J.A., Gong, Q., 2013. Anatomical and functional brain abnormalities in drug-naive first-episode schizophrenia. American Journal of Psychiatry 170, 1308-1316.

Reuter, M., Fischl, B., 2011. Avoiding asymmetry-induced bias in longitudinal image processing. Neuroimage 57, 19-21.

Richard, A.E., Carter, C.S., Cohen, J.D., Cho, R.Y., 2013. Persistence, diagnostic specificity and genetic liability for context-processing deficits in schizophrenia. Schizophrenia Research 147, 75-80.

Schmahmann, J.D., 2001. The cerebrocerebellar system: anatomic substrates of the cerebellar contribution to cognition and emotion. International Review of Psychiatry 13, 247-260.

Shen, H., Wang, L., Liu, Y., Hu, D., 2010. Discriminative analysis of resting-state functional connectivity patterns of schizophrenia using low dimensional embedding of fMRI. Neuroimage 49, 3110-3121.

Song, H., Bogdan, I.I.M., Wang, S., Dong, W., Quan, W., Dang, W., Yu, X., 2017. Automatic schizophrenia discrimination on fNIRS by using PCA and SVM. IEEE International Conference on Bioinformatics and Biomedicine, pp. 389-394.

Su, L., Li, T., Deng, W., Jiang, L., Wu, Q., Tang, H., Yue, Q., Huang, X., Chan, R.C., Collier, D.A., 2010. Short-term Effects of Antipsychotic Treatment on Cerebral Function in Drug-Naive First-Episode Schizophrenia Revealed by “Resting State” Functional Magnetic Resonance Imaging. Archives of General Psychiatry 67, 783.

Su, L., Wang, L., Shen, H., Feng, G., Hu, D., 2013. Discriminative analysis of non-linear brain connectivity in schizophrenia: an fMRI Study. Front Hum Neurosci 7, 702.

Sui, J., Castro, E., He, H., Bridwell, D., Du, Y., Pearlson, G.D., Jiang, T., Calhoun, V.D., 2014. Combination of FMRI-SMRI-EEG data improves discrimination of schizophrenia patients by ensemble feature selection. Engineering in Medicine and Biology Society, pp. 3889-3892.

Sui, J., He, H., Yu, Q., Chen, J., Rogers, J., Pearlson, G.D., Mayer, A., Bustillo, J., Canive, J., Calhoun, V.D., 2013. Combination of Resting State fMRI, DTI, and sMRI Data to Discriminate Schizophrenia by N-way MCCA + jICA. Front Hum Neurosci 7, 235.

Sweeney, E.M., Vogelstein, J.T., Cuzzocreo, J.L., Calabresi, P.A., Reich, D.S., Crainiceanu, C.M., Shinohara, R.T., 2014. A comparison of supervised machine learning algorithms and feature vectors for MS lesion segmentation using multimodal structural MRI. PLoS One 9, e95753.

Teipel, S., Drzezga, A., Grothe, M.J., Barthel, H., Chã©Telat, G., Schuff, N., Skudlarski, P., Cavedo, E., Frisoni, G.B., Hoffmann, W., 2015. Multimodal imaging in Alzheimer's disease: validity and usefulness for early detection. Lancet Neurology 14, 1037-1053.

Tibshirani, R., 2011. Regression Shrinkage and Selection via the Lasso. Journal of the Royal Statistical Society: Series B (Statistical Methodology) 73, 267-288.

Wang, H., Guo, W., Feng, L., Wang, G., Lyu, H., Wu, R., Chen, J., Shuai, W., Li, L., Zhao, J., 2016. Patients with first-episode, drug-naive schizophrenia and subjects at ultra-high risk of psychosis shared increased cerebellar-default mode network connectivity at rest. Sci Rep 6, 26124.

Wang, Q., Cheung, C., Deng, W., Li, M., Huang, C., Ma, X., Wang, Y., Jiang, L., Sham, P.C., Collier, D.A., 2013. White-matter microstructure in previously drug-naive patients with schizophrenia after 6 weeks of treatment. Psychological Medicine 43, 2301-2309.

Wee, C.Y., Yap, P.T., Zhang, D., Denny, K., Browndyke, J.N., Potter, G.G., Welsh-Bohmer, K.A., Wang, L., Shen, D., 2012. Identification of MCI individuals using structural and functional connectivity networks. Neuroimage 59, 2045-2056.

Wright, J., Ganesh, A., Zhou, Z., Wagner, A., Ma, Y., 2009. Demo: Robust face recognition via sparse representation. IEEE International Conference on Automatic Face & Gesture Recognition, pp. 1-2.

Yang, H., He, H., Zhong, J., 2016. Multimodal MRI characterisation of schizophrenia: a discriminative analysis. The Lancet 388, S36.

Yu, Y., Shen, H., Zeng, L.L., Ma, Q., Hu, D., 2013a. Convergent and Divergent Functional Connectivity Patterns in Schizophrenia and Depression. PLoS One 8, e68250.

Yu, Y., Shen, H., Zhang, H., Zeng, L.L., Xue, Z., Hu, D., 2013b. Functional connectivity-based signatures of schizophrenia revealed by multiclass pattern analysis of resting-state fMRI from schizophrenic patients and their healthy siblings. Biomed Eng Online 12, 10.

Zeng, B., Ardekani, B.A., Tang, Y., Zhang, T., Zhao, S., Cui, H., Fan, X., Zhuo, K., Li, C., Xu, Y., 2016. Abnormal white matter microstructure in drug-naive first episode schizophrenia patients before and after eight weeks of antipsychotic treatment. Schizophrenia Research 172, 1-8.

Zhang, D., Wang, Y., Zhou, L., Yuan, H., Shen, D., 2011a. Multimodal classification of Alzheimer's disease and mild cognitive impairment. Neuroimage 55, 856.

Zhang, D., Wang, Y., Zhou, L., Yuan, H., Shen, D., 2011b. Multimodal classification of Alzheimer's disease and mild cognitive impairment. Neuroimage 55, 856-867.

Zhou, Y., Shu, N., Liu, Y., Song, M., Hao, Y., Liu, H., Yu, C., Liu, Z., Jiang, T., 2008. Altered resting-state functional connectivity and anatomical connectivity of hippocampus in schizophrenia. Schizophrenia Research 100, 120-132.